

PERFORMANCE DEGRADATION ASSESSMENT METHOD FOR AERO-ENGINES ACROSS THE FULL LIFE-CYCLE BASED ON DIGITAL TWIN

Zilang Huang[1,2,3], Dasheng Xiao[1,2,3], Xiaofan Guo[1,2,3], Le Zhao[1,2,3] & Chenchen Song[1,2,3]

[1]School of Power and Energy, Northwestern Polytechnical University, 710072, Xi'an, Shaanxi, PR China
[2]National Key Laboratory of Science and Technology on Advanced Light-duty Gas-turbine, PR China
[3]Key Laboratory of Digital and Intelligent Technologies for Aero-engine, Ministry of Industry and Information Technology, Xi'an 710072, China

Abstract

Accurate performance degradation monitoring is essential for ensuring aero-engine operational safety, supporting condition-based maintenance, and preventing performance deterioration from evolving into severe faults. Performance degradation monitoring for aero-engines is challenging under varying operating conditions, where environmental and control variations can obscure degradation-induced performance changes. To address this issue, this paper proposes a same-condition performance degradation monitoring framework that quantifies degradation by comparing healthy baseline performance with real-time operating performance under identical operating conditions. A Baseline-State Model (BLS model) is developed to reconstruct the healthy reference performance, while a Real-time Performance Model estimates the current operating performance. Both models incorporate aero-engine physical structural priors and employ bidirectional long short-term memory (BiLSTM) networks; the Real-time model further uses multi-head self-attention to capture component-level temporal degradation features. Experiments on the National Aeronautics and Space Administration (NASA) New Commercial Modular Aero-Propulsion System Simulation (N-CMAPSS) DS02 dataset show that the BLS model achieves a mean absolute relative error (MARE) of $\mu_{\mathrm{MARE}} < 0.2\%$, while the Real-time model maintains $\mu_{\mathrm{MARE}} < 0.4\%$. The resulting degradation trends are consistent with aero-engine degradation behavior, indicating that the proposed framework can effectively support same-condition performance degradation monitoring under varying operating conditions.

Keywords: Aero-engines, Performance degradation, Self-attention mechanism, Digital twin, Bidirectional long short-term memory (BiLSTM)

1. Introduction

Aero-engines are core components of aircraft, and their performance condition is directly related to flight safety, mission reliability, and maintenance decision-making. With increasing operating time, key gas-path components, such as compressors, combustors, and turbines, gradually degrade under complex loads, thermal cycles, and varying operating conditions. This degradation causes performance parameters, including pressure, temperature, and efficiency, to deviate from their healthy-state values [1, 2, 3]. Therefore, accurately monitoring aero-engine performance condition and degradation severity under varying operating conditions is of great importance for safety warning, performance optimization, and service-life extension [4, 5, 6].

However, performance degradation assessment differs from conventional performance parameter prediction. During actual flight, environmental variables and control inputs, such as altitude, Mach number, inlet temperature, and throttle lever angle, vary continuously. Consequently, measured performance parameters are affected by both operating-condition variations and component degradation

[7, 8]. A rigorous degradation assessment should therefore compare the current operating performance with the healthy reference performance under the same operating condition.

Existing methods for aero-engine performance assessment and degradation monitoring can be broadly classified into mechanism-based models, data-driven models, and physics-data hybrid models [9, 10]. Mechanism-based models offer strong interpretability but are often limited by model mismatch, unmeasurable parameters, and simplifying assumptions [11, 12, 13, 14]. Data-driven models can characterize complex nonlinear relationships [15], but they lack explicit physical constraints and may degenerate into black-box predictors. Physics-data hybrid models improve prediction accuracy and robustness by incorporating physical knowledge [16, 17]. Nevertheless, most existing methods introduce physical knowledge as external constraints, loss terms, or auxiliary modules, while insufficiently exploiting structural priors related to engine component architecture, inter-component coupling, and gas-path propagation routes.

To overcome the interference of operating-condition variations and the insufficient use of engine structural priors in existing methods, this paper proposes a same-condition performance degradation assessment framework incorporating aero-engine physical structural priors. The framework quantifies degradation by comparing the reconstructed healthy reference performance and the estimated real-time operating performance under identical operating conditions. To achieve this, a Baseline-State Model and a Real-time Performance Model are developed, both of which embed engine component topology and gas-path propagation relationships to improve prediction accuracy and physical interpretability.

The remainder of this paper is organized as follows. Section 2 presents the computation method for aero-engine performance degradation under the same operating condition and describes the physical knowledge embedded in the network. Section 3 details the architectures of the BLS model and the Real-time Performance Model. Section 4 validates the prediction accuracy of the models and the effectiveness of the proposed performance degradation computation method using the National Aeronautics and Space Administration (NASA) New Commercial Modular Aero-Propulsion System Simulation (N-CMAPSS)simulation dataset.

2. Problem Formulation and Physics-Embedded Framework

2.1 Formulation of Engine Performance Degradation

According to aero-engine operating principles, the engine operating state is jointly determined by environmental parameters X_{env} and control parameters X_{control} [16]. When the environmental conditions and control inputs at two different time instants are identical, the engine can be regarded as operating under the same condition. Under this constraint, variations in engine-level performance parameters mainly reflect the effects of internal component degradation.Let $Y^{\text{target}}_{\text{performance}}(t_i)$ denote the target engine-level performance parameter at time t_i, and let $Y^{\text{target}}_{\text{performance}}(t_0)$ denote the corresponding healthy baseline performance under the same operating condition. The engine performance degradation magnitude is defined as the relative performance deviation between the healthy reference state and the current operating state:

$$
\begin{aligned}
D(t_i) &= \frac{Y^{\text{target}}_{\text{performance}}(t_0) - Y^{\text{target}}_{\text{performance}}(t_i)}{Y^{\text{target}}_{\text{performance}}(t_0)} \times 100\%, \\
\text{s.t.} \quad & \begin{cases} X_{\text{env}}(t_0) = X_{\text{env}}(t_i), \\ X_{\text{control}}(t_0) = X_{\text{control}}(t_i). \end{cases}
\end{aligned}
\tag{1}
$$

This constraint requires the healthy reference state and the current operating state to correspond to exactly the same operating condition.

In practice, it is extremely difficult to fully satisfy these two constraints. For instance, it is impossible to ensure that the engine operates under identical conditions—such as altitude, ambient temperature, and humidity—throughout its entire service life, particularly during full afterburner states. Moreover, during the full life cycle of the engine, certain key performance parameters are either unmeasurable or cannot be measured with sufficient accuracy in flight. A typical example is thrust, which is notoriously difficult to measure precisely during actual operation, thereby posing a significant challenge

to accurate assessment of overall engine performance degradation. From the above analysis, two major challenges in current performance degradation monitoring can be identified:

- It is nearly impossible to maintain exactly the same operating conditions as those at the engine's initial state at any arbitrary moment during future operation, making it impossible to directly calculate performance degradation solely from sensor measurements.
- Several critical performance parameters essential for evaluating overall engine health are either unmeasurable or difficult to measure accurately in real-world operating environments.

To address these two challenges, this study develops two types of digital twin models: the Baseline State Performance Prediction Model (BLS Model) and the Real-time Performance Prediction Model (Real-time Model).
The overall workflow of the engine performance degradation monitoring method based on these two models is illustrated in Figs 1. Specifically, the two digital twin models (BLS and Real-time) are first established. Then, at every future operating moment, both models are executed under identical digitized test conditions . This yields: (1) the baseline performance that the engine would theoretically achieve at that moment in its initial healthy state, and (2) the real-time performance exhibited by the degraded engine. By comparing the baseline performance with the real-time performance, the current performance degradation of the engine is quantitatively assessed in real time.

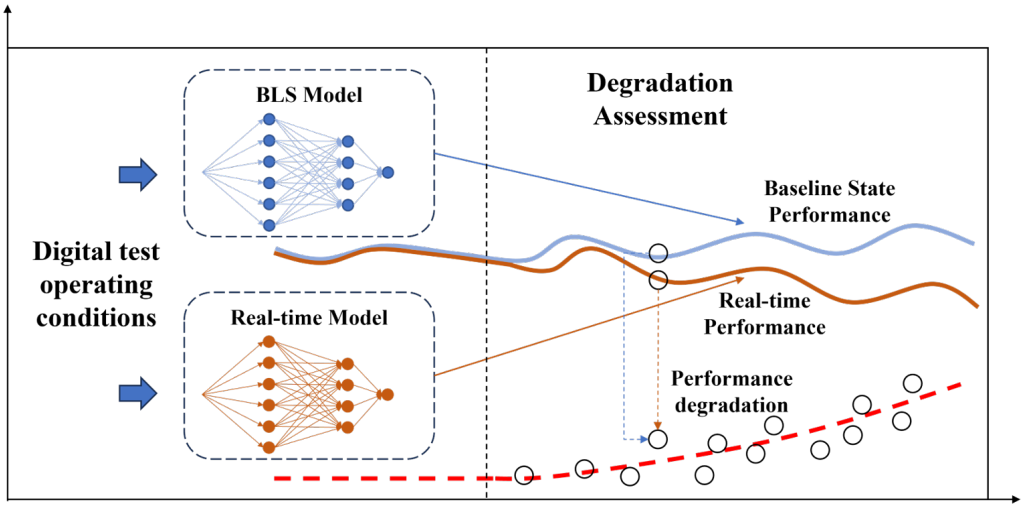


Figure 1 – Engine Performance Degradation Assessment Method Based on Two Types of Digital Twin Models.

2.2 Physics-Embedded Data–Knowledge Hybrid Framework

The predictions of the BLS model and the Real-time model jointly determine the final performance degradation magnitude. Therefore, both models should achieve high prediction accuracy while remaining consistent with the actual operating mechanisms of aero-engines. Although conventional end-to-end neural networks can approximate nonlinear relationships between input variables and performance parameters, they often neglect thermodynamic coupling and directed propagation among gas-path components, resulting in black-box mappings with limited physical interpretability. Since local component-level performance changes propagate progressively along the gas-path structure and are eventually reflected in engine-level performance parameters, incorporating physical structural priors into the model architecture is essential for improving the reliability and interpretability of degradation assessment.
Motivated by these characteristics, this study adopts a physics–data hybrid modeling strategy and embeds aero-engine structural priors into the neural network topology [18, 19]. Specifically, three types of embeddable physical knowledge are considered. The first is component functional decomposition: an aero-engine consists of functional components, including the fan, compressor, combustor,

turbine, and exhaust nozzle, each corresponding to a distinct thermodynamic process. The second is component matching relationships, where different components are coupled through shafts, mass-flow continuity, and energy transfer. For example, the high-pressure compressor and high-pressure turbine share the high-pressure shaft speed, whereas the fan, low-pressure compressor, and low-pressure turbine share the low-pressure shaft speed. The third is gas-path topological propagation, in which airflow is transmitted sequentially from upstream to downstream components along the engine gas path.

In the network implementation, these three types of physical knowledge are mapped to modular decomposition, shared inputs, and data-flow connections, respectively. Component-specific subnetworks are first constructed according to the main gas-path components, so that each subnetwork has a clear physical meaning. Key operating variables are then shared across relevant subnetworks to represent component matching relationships. Finally, feature-transfer paths are established following the gas-path propagation direction, allowing upstream subnetwork outputs to serve as part of the inputs to downstream subnetworks.

In this manner, the proposed method does not forcibly impose complete mechanistic equations on the neural network. Instead, it transforms aero-engine physical structure into network-topology priors, thereby introducing physics-consistent constraints into data-driven modeling and improving model interpretability and adaptability under complex operating conditions.

3. Physics-Embedded Degradation Monitoring Method

Within the component-specific subnetworks, bidirectional long short-term memory (BiLSTM) modules are employed to extract temporal features from historical operating sequences. Compared with a unidirectional long short-term memory moddules (LSTM) [20], BiLSTM can exploit both forward and backward temporal dependencies within the observation window, which is beneficial for characterizing local performance evolution under varying operating conditions. To further emphasize the influence of informative historical time steps on current performance prediction, the Real-time Performance Model incorporates a multi-head self-attention mechanism [21] into the component subnetworks.The structure of the multi-head self-attention mechanism is illustrated in Fig. 2. This mechanism adaptively reweights time-step features, and a residual connection is used to fuse the attention-enhanced features with the original temporal features. In this way, the continuity of performance evolution is preserved while the stability of model training is improved.

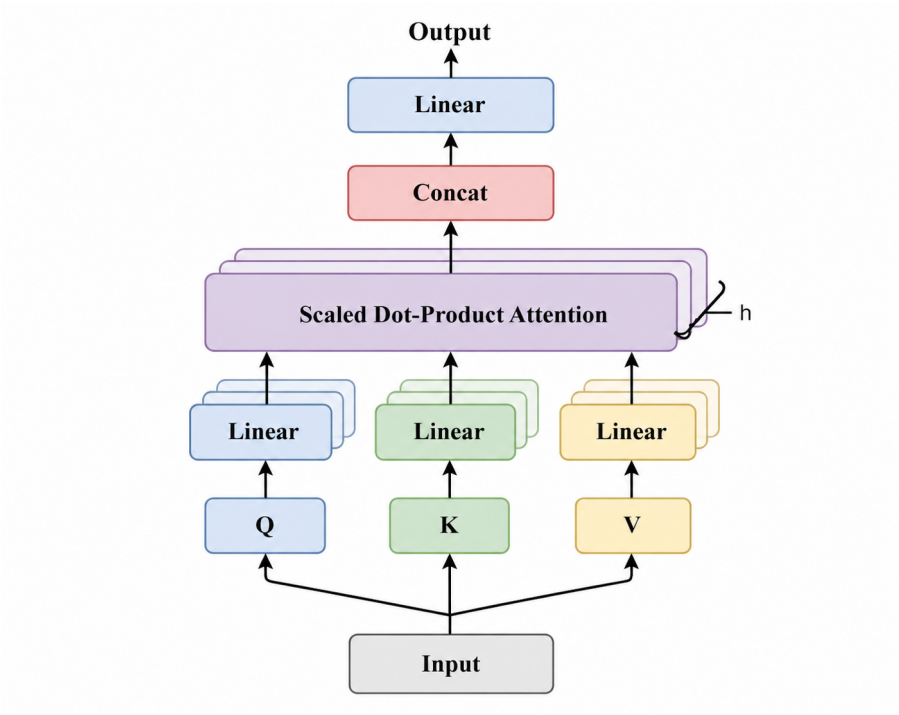


Figure 2 – Architecture of the Multi-Head Self-Attention Model.

3.1 Baseline-State Model

The Baseline-State Model (BLS Model) is designed to reconstruct the healthy-state performance corresponding to the current operating condition. Its inputs include only the environmental variables $X_{\text{env}}(t_i)$ and control variables $X_{\text{control}}(t_i)$, and its output is the healthy baseline value of the target performance parameter, denoted as $Y_0^{\text{target}}(t_i)$. Since the model is trained using data from the initial healthy stage, it learns the mapping between operating-condition variables and performance parameters under approximately healthy operating conditions.

$$Y_0^{\text{target}}(t_i) = M_0\left(X_{\text{env}}(t_i), X_{\text{control}}(t_i)\right) \tag{2}$$

where $Y_0^{\text{target}}(t_i)$ denotes the healthy baseline performance reconstructed by the BLS Model under the current operating condition, and M_0 represents the baseline performance model trained using data from the initial healthy stage.

Figure 3 illustrates the architecture of the proposed BLS Model. In the network implementation, operating-condition variables are first organized according to the physical topology of the aero-engine components and are then fed into the performance mapping network. This design establishes a nonlinear mapping between operating-condition parameters and healthy baseline performance while maintaining consistency with the physical structure of the engine.

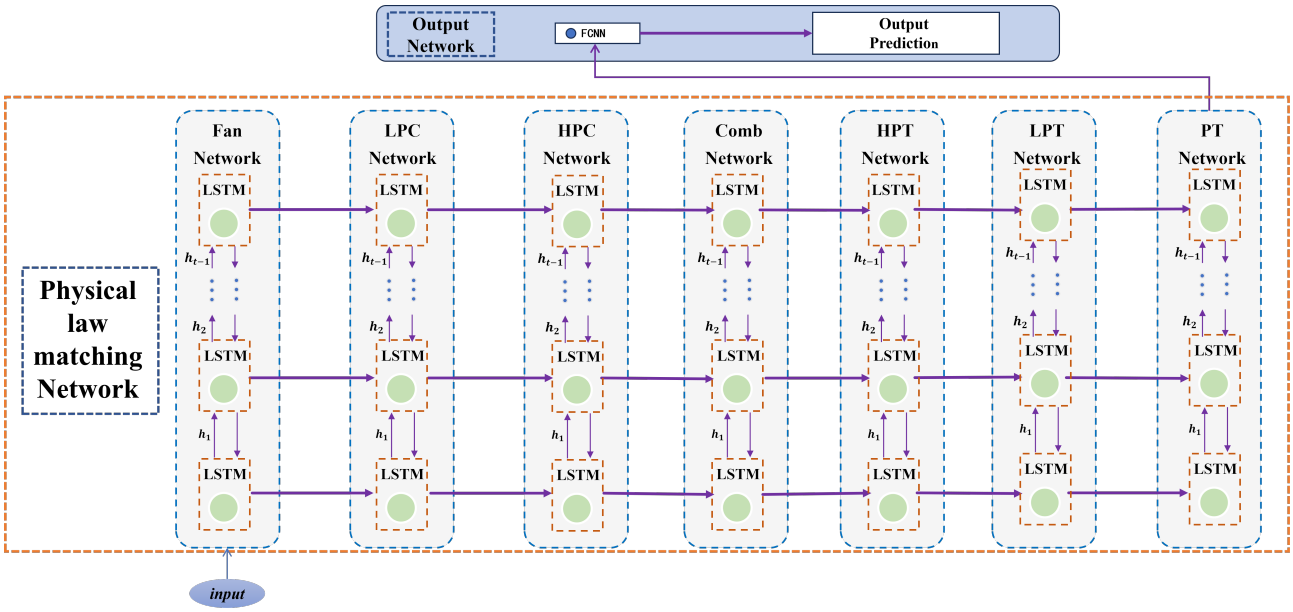


Figure 3 – Architecture of the BLS Model.

3.2 Real-time Model

Unlike the BLS Model, which uses only environmental and control parameters as inputs, the Real-time model further incorporates measurable sensor parameters or auxiliary state parameters $S(t_i)$ that are correlated with the target performance parameter, in addition to $X_{\text{env}}(t_i)$ and $X_{\text{control}}(t_i)$. Here, $S(t_i)$ does not include the target performance parameter to be predicted. The Real-time model can be expressed as

$$Y_{\text{R}}^{\text{target}}(t_i) = M_{\text{R}}\left(X_{\text{env}}(t_i), X_{\text{control}}(t_i), S(t_i)\right) \tag{3}$$

where M_{R} denotes the Real-time model, and $Y_{\text{R}}^{\text{target}}(t_i)$ represents the real-time target performance parameter of the engine at time t_i estimated by the model.

Figure 4 shows the structure of the Real-time model constructed in this paper. The model consists of a physical-rule matching network, a temporal feature extraction module, a self-attention enhancement module, and a performance mapping network. The physical-rule matching network organizes the input features at the component level according to the aero-engine gas-path topology. The temporal feature extraction module extracts performance evolution information from historical operating

sequences. The self-attention enhancement module highlights key historical information that is more relevant to the current performance prediction. The performance mapping network outputs the real-time performance estimation result at the current time.

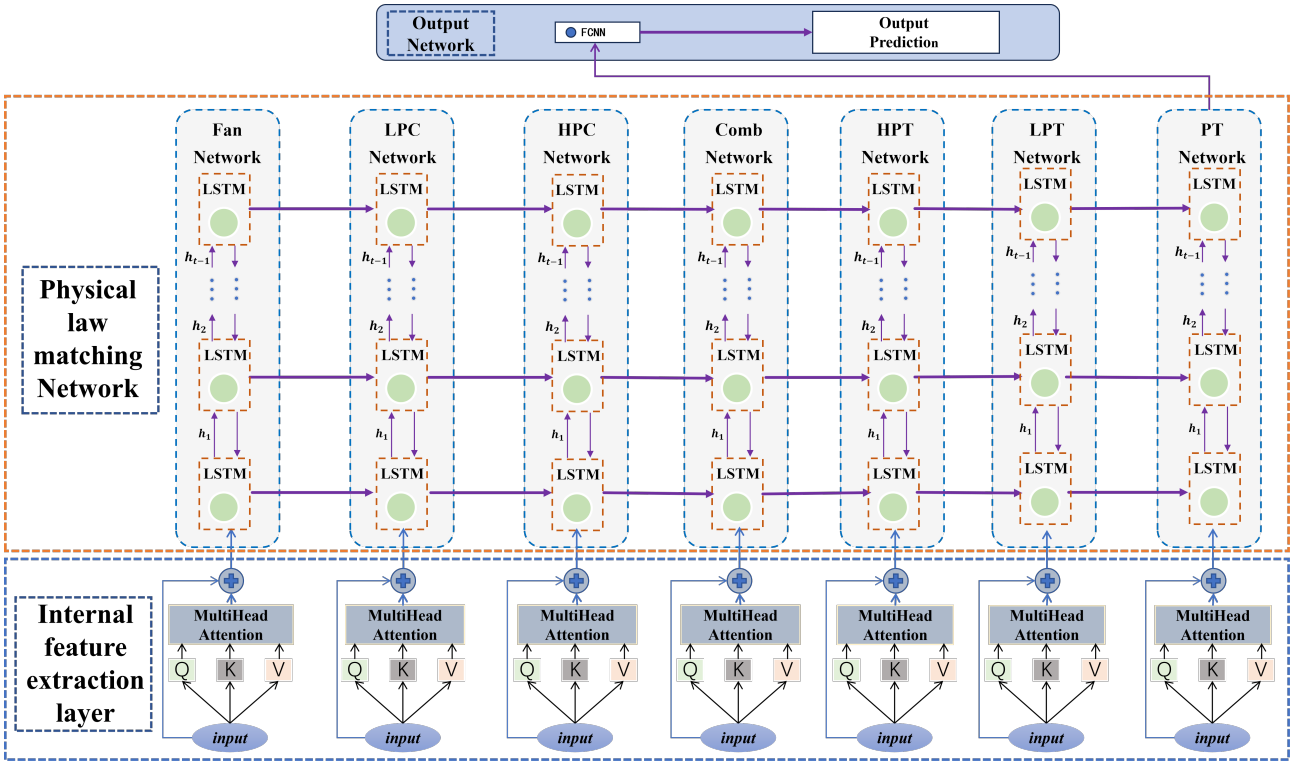


Figure 4 – Architecture of the Real Model.

4. Case Study

4.1 Data Processing

To validate the effectiveness of the proposed performance degradation monitoring method, this paper conducts a case study using the DS02 subset of the NASA N-CMAPSS dataset. DS02 contains full-life-cycle simulated degradation data for nine engines from healthy to failure states. Its operating conditions are derived from real engine flight profiles, with component degradation modes further introduced. Therefore, this subset is suitable for aero-engine performance degradation monitoring and assessment. In this paper, data from six engines are selected as the training set, while data from the remaining three engines are used as the test set. The degraded components of each engine and the data split are shown in Table 1, and the recorded parameters in the dataset are listed in Table 2.

Dataset split	Engine ID	Data size (MB)	Total flight cycles	Flight class	Degraded components
Training dataset	2	0.85	75	FC3	HPT
	5	1.03	89	FC3	HPT
	10	0.95	82	FC3	HPT
	16	0.77	63	FC3	HPT, LPT
	18	0.89	71	FC3	HPT, LPT
	20	0.77	66	FC3	HPT, LPT
Testing dataset	11	0.66	59	FC3	HPT, LPT
	14	0.16	76	FC1	HPT, LPT
	15	0.43	67	FC2	HPT, LPT

Table 1 – Data-related information of the nine engines in the DS02 subset.

Category	No.	Parameter	Symbol	Unit
Operating-state parameters X_W	1	Flight altitude	H	ft
	2	Flight Mach number	Ma	-
	3	Throttle lever angle	PLA	%
	4	Fan inlet total temperature	$T_{t,2}$	$^\circ R$
Measurable sensor parameters X_S	5	Fan physical speed	Nf	rpm
	6	Core physical speed	Nc	rpm
	7	Fuel flow rate	W_f	pps
	8	LPC outlet total temperature	$T_{t,24}$	$^\circ R$
	9	HPC outlet total temperature	$T_{t,30}$	$^\circ R$
	10	HPT outlet total temperature	$T_{t,48}$	$^\circ R$
	11	LPT outlet total temperature	$T_{t,50}$	$^\circ R$
	12	Bypass duct total pressure	$P_{t,15}$	psia
	13	Fan inlet total pressure	$P_{t,2}$	psia
	14	Fan outlet total pressure	$P_{t,21}$	psia
	15	LPC outlet total pressure	$P_{t,24}$	psia
	16	HPC outlet static pressure	$P_{s,30}$	psia
	17	Combustor outlet total pressure	$P_{t,40}$	psia
	18	LPT outlet total pressure	$P_{t,50}$	psia

Table 2 – Parameter-related information used for performance degradation monitoring.

4.1.1 Training Data Selection for the BLS Model

For the 13 performance-state-related parameters, a corresponding BLS Model is constructed for each parameter. The inputs include only environmental and control parameters, namely flight altitude, flight Mach number, fan inlet total temperature, and throttle lever angle, while the output is the corresponding target performance parameter. To ensure that the BLS Model learns the mapping relationship between operating-condition parameters and performance parameters under healthy conditions, this paper selects data from the climb and cruise phases within the first 10 flight cycles of each of the six training engines as training samples. This stage is approximately regarded as the initial healthy stage of the engine. In the testing stage, data from the same flight phases within the first 10 flight cycles of the remaining three test engines are selected to evaluate the ability of the BLS Model to reconstruct healthy baseline performance.

4.1.2 Training Data Selection for the Real-time Model

For the Real-time model, measurable performance parameters related to the target performance parameter are introduced as auxiliary inputs. To avoid the subjectivity caused by manual input-variable selection, this paper uses the Spearman rank correlation coefficient to analyze the correlations among the 13 performance-related parameters. The calculation formula is given as follows:

$$\rho = 1 - \frac{6\sum_{i=1}^{n} d_i^2}{n(n^2-1)} \tag{4}$$

where n is the number of samples, and d_i denotes the rank difference between the two variables for the i-th sample. A value of $|\rho|$ closer to 1 indicates a stronger monotonic correlation between the two parameters.

To avoid information leakage from the test set, parameter correlations are calculated only using the training set. For each target performance parameter, other performance parameters with an absolute Spearman correlation coefficient no less than 0.9 are selected as auxiliary input variables for the Real-time model. The correlation analysis results are shown in Fig. 5. To enable the Real-time model to fully learn the performance evolution patterns over the full life cycle of aero-engines, this paper selects the full-life-cycle data of the six training engines as training samples, while retaining

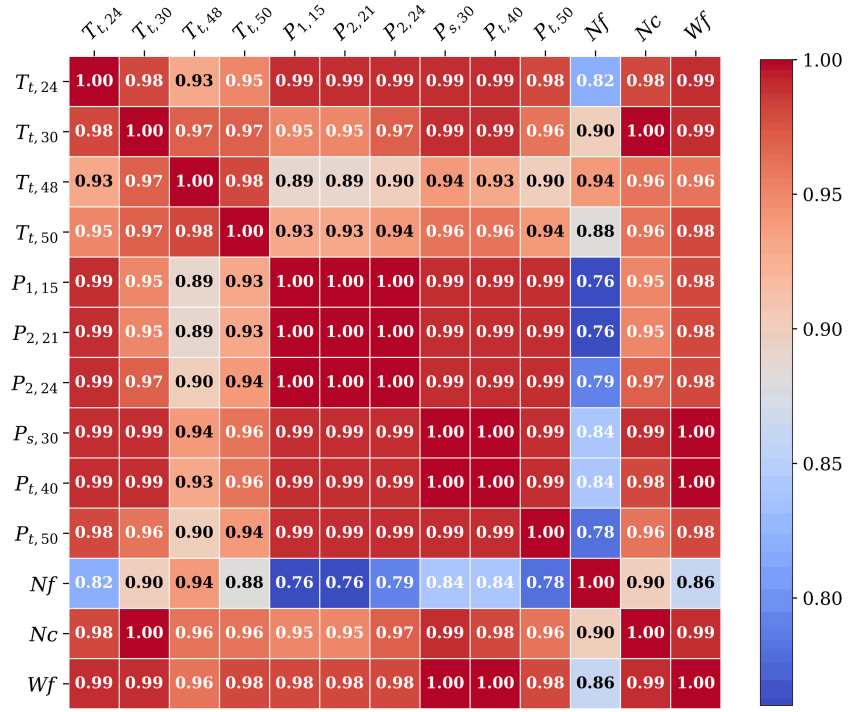


Figure 5 – Correlation heatmap of the 13 performance-related parameters.

only the climb and cruise phases. In the testing stage, the full-life-cycle data of the remaining three engines are used for model evaluation.

4.2 Model Training

Before model training, Min–Max normalization is applied to both input and output variables to unify their scales, and inverse normalization is performed after prediction to recover the original physical dimensions. Considering the temporal characteristics of aero-engine operating data, a sliding-window strategy is used to construct model input samples. The window length and sliding step are set to 4 and 1, respectively. The data of each engine are sliced independently to avoid mixing sequences from different engines. The model hyperparameters are determined based on preliminary tuning results and experience from related studies [16], with the specific configuration listed in Table 7. During training, MSE is used as the loss function, and the Adam optimizer is employed for parameter updates. The learning rate, batch size, and number of training epochs are set to 0.001, 256, and 200, respectively. To reduce the influence of random initialization on the results, each model is trained five times, and model performance is evaluated based on the results of multiple experiments. All experiments are implemented in Python 3.8 and conducted on an NVIDIA GeForce RTX 3070 Laptop GPU.

4.3 Results of the Case Study

This section evaluates the prediction accuracy of the trained 13 BLS Models and their corresponding Real-time models. After comparing the prediction accuracy of each model, the BLS Model and Real-time model with the best performance for each target performance parameter are selected as the base models for subsequent performance degradation calculation.

4.3.1 Prediction Accuracy of the BLS Model

In this study, the mean absolute relative error (MARE) is used to evaluate the single-run accuracy of each model. The average MARE of each model over five testing runs is used to evaluate the accuracy of the BLS Model for the corresponding performance parameter. The calculation formulas are as follows:

$$\mathrm{MARE} = \frac{1}{n}\sum_{i=1}^{n}\left|\frac{y_i^{\text{prediction}} - y_i^{\text{experimental}}}{y_i^{\text{experimental}}}\right| \times 100\% \tag{5}$$

$$\mu_{\mathrm{MARE}} = \frac{1}{5}\sum_{i=1}^{5}\mathrm{MARE}_i \tag{6}$$

where $y_i^{\text{prediction}}$ denotes the predicted value of the model at the i-th test sample, and $y_i^{\text{experimental}}$ denotes the actual monitored value at the i-th sample in the test dataset. MARE represents the mean absolute relative error over all samples in the test set for each testing run, and μ_{MARE} represents the average value of MARE over five testing runs for each model. A MARE value closer to 0 indicates higher accuracy of the model used in the corresponding testing run, while a μ_{MARE} value closer to 0 indicates higher overall accuracy of this type of model.

The test results of the BLS Models corresponding to different performance parameters are shown in Fig. 6, Fig. 7, Fig. 8. It can be observed that, on the initial 10 flight cycles of the three test engines, most MARE values of the BLS Models corresponding to the 13 performance parameters are below 0.20%. This indicates that the constructed BLS Models can accurately reconstruct the baseline performance parameters of the engine in the initial healthy state, thereby providing reliable healthy reference baselines for subsequent performance degradation calculation.

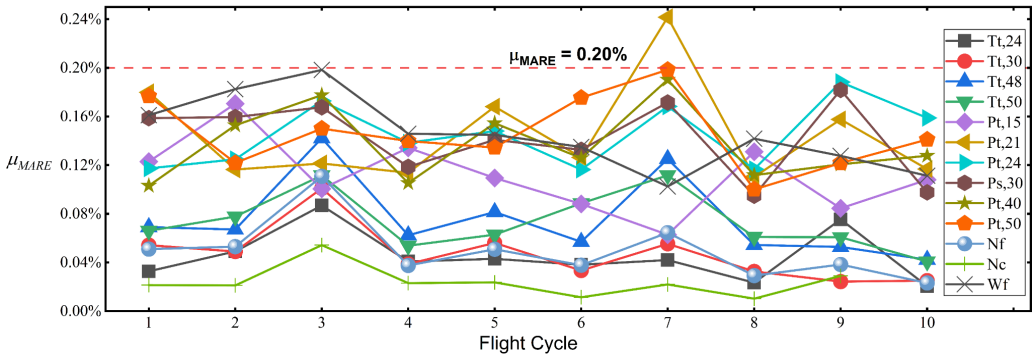


Figure 6 – Test results of the BLS model on the first 10 flight cycles of test engine No. 11.

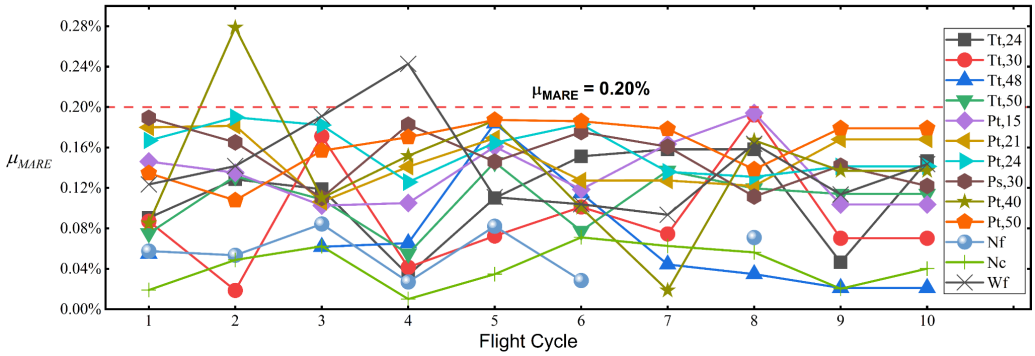


Figure 7 – Test results of the BLS model on the first 10 flight cycles of test engine No. 14.

4.3.2 Prediction Accuracy of the Real-time Model

For the Real-time models corresponding to different performance parameters, this paper further evaluates their prediction accuracy over the full life cycle and adopts MARE as the evaluation metric. The test results are shown in Fig. 9, Fig. 10, and Fig. 11.

The results show that, on the full-life-cycle data of test engine No. 11and No. 15, the MARE values of the Real-time models corresponding to the 13 performance parameters are generally below 0.30%, with most parameters below 0.20%. For the No. 14 test engines, the MARE values are generally below 0.40%. These results indicate that the constructed Real-time models can accurately characterize the real-time performance condition of aero-engines over the full life cycle, thereby providing reliable performance estimation results for subsequent performance degradation calculation.

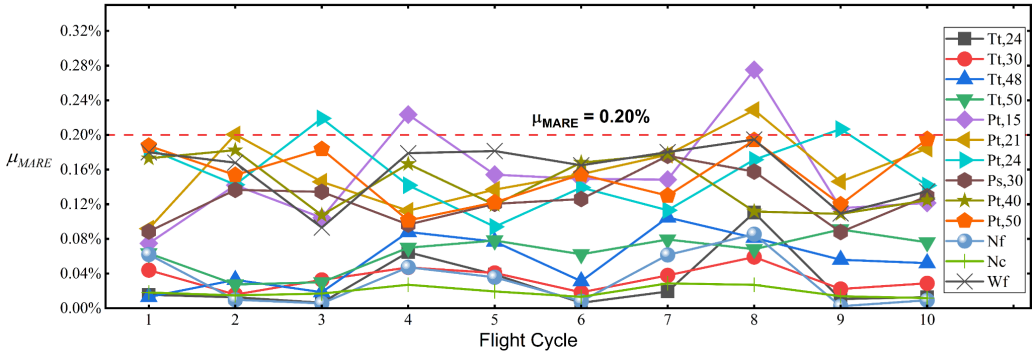


Figure 8 – Test results of the BLS model on the first 10 flight cycles of test engine No. 15.

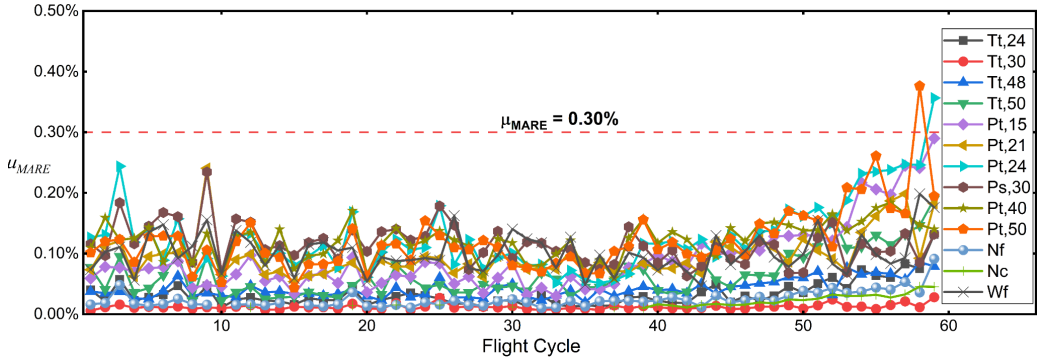


Figure 9 – Test results of the Real-time model on the first 10 flight cycles of test engine No. 11.

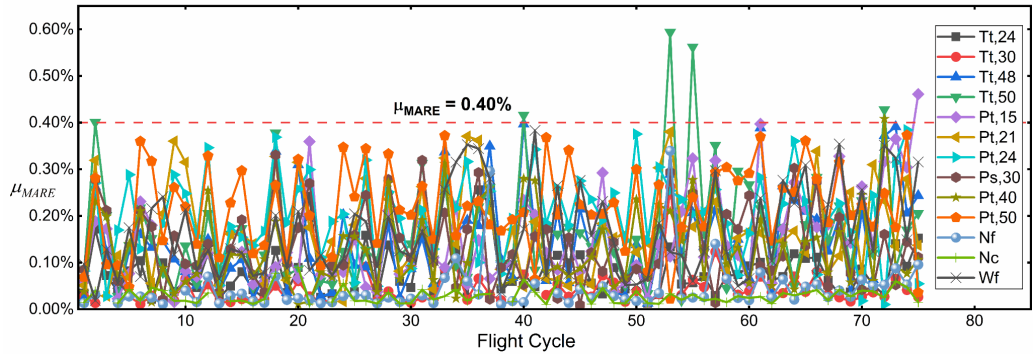


Figure 10 – Test results of the Real-time model on the first 10 flight cycles of test engine No. 14.

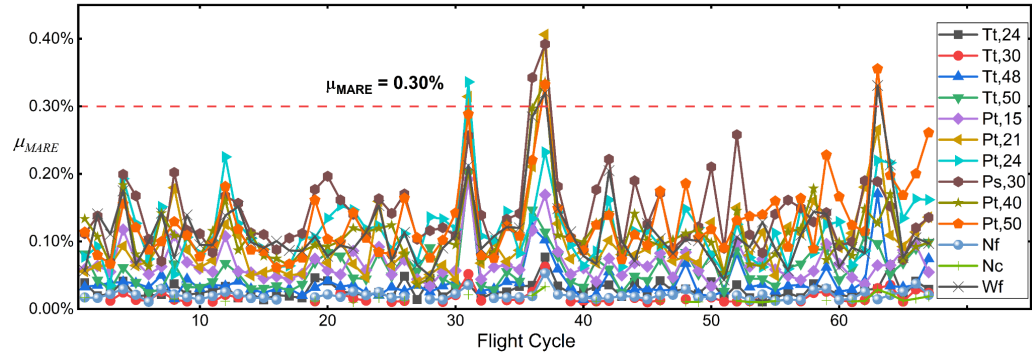


Figure 11 – Test results of the Real-time model on the first 10 flight cycles of test engine No. 15.

4.3.3 Engine Performance Degradation Calculation Results

For the above 13 performance parameters, the optimal BLS Model and Real-time model corresponding to each parameter are selected for performance degradation assessment. The BLS Model reconstructs the healthy baseline performance under the current operating condition, and the Real-time model estimates the real-time engine performance. The performance degradation at each sample point is then calculated according to Eq. (1). For a single flight cycle, the average degradation value of all sample points within that cycle is further calculated and regarded as the overall performance degradation of the corresponding flight cycle. By arranging the degradation values of all flight cycles in chronological order, the degradation curve of the corresponding performance parameter over the full life cycle of the engine can be obtained.

Taking test engine No. 11 as an example, its full life cycle contains 59 flight cycles. According to the above method, the degradation curves of its 13 performance parameters over the full life cycle can be obtained. Performance degradation assessment is conducted separately for the three test engines, and the results are shown in Fig. 12, Fig. 13, Fig. 14.

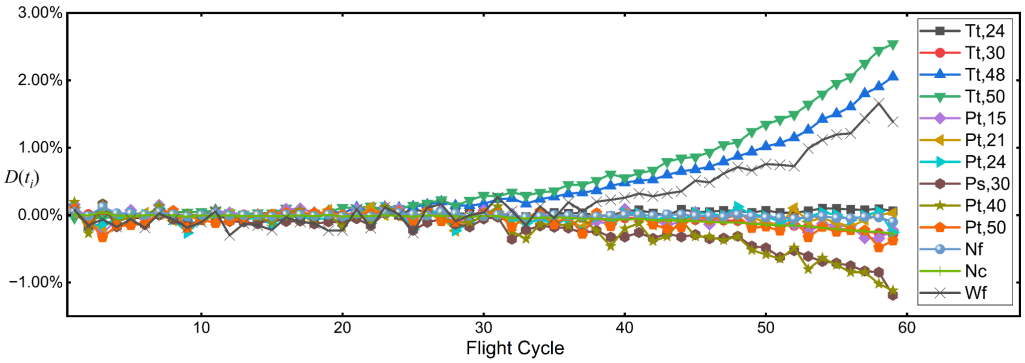


Figure 12 – Performance degradation assessment results of test engine No. 11 over its full life cycle.

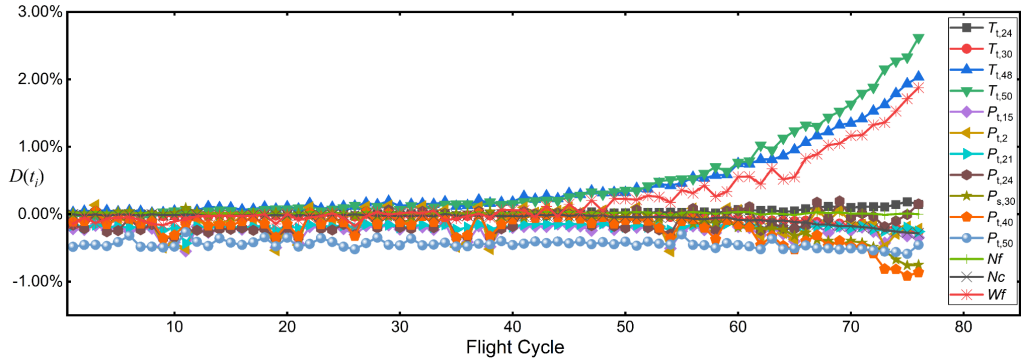


Figure 13 – Performance degradation assessment results of test engine No. 14 over its full life cycle.

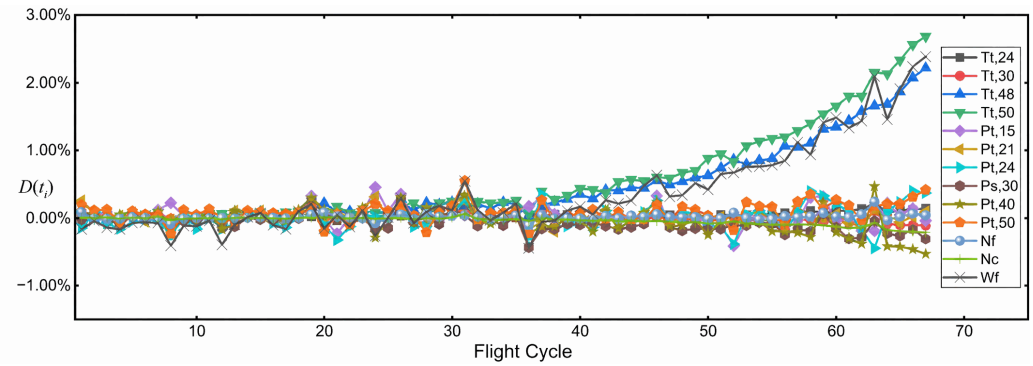


Figure 14 – Performance degradation assessment results of test engine No. 15 over its full life cycle.

It can be observed that most performance parameters gradually deviate from the healthy baseline state as the number of flight cycles increases, and the absolute degradation magnitude generally increases with operating time. A negative degradation value indicates that the corresponding performance parameter gradually decreases relative to the healthy baseline value, whereas a positive degradation value indicates that the parameter gradually increases relative to the healthy baseline value. Specifically, $T_{t,48}$, $T_{t,50}$, and W_f show clear increasing trends, while $P_{t,40}$ and $P_{s,30}$ exhibit relatively obvious decreasing trends.

Furthermore, this paper calculates the performance degradation values of the three test engines at the final flight cycle, as shown in Table 3. It can be found that some parameters have relatively small final degradation values and show no obvious trend over the full life cycle. This indicates that these parameters do not exhibit significant degradation characteristics under the corresponding degradation modes, and the small calculated variations may mainly originate from model prediction errors, such as the N_f parameter.

Parameter	Engine No. 11	Engine No. 14	Engine No. 15
$T_{t,24}$	0.162%	0.141%	0.159%
$T_{t,30}$	-0.268%	-0.255%	-0.151%
$T_{t,48}$	2.131%	2.048%	2.259%
$T_{t,50}$	2.513%	2.589%	2.374%
$P_{t,15}$	-0.236%	-0.354%	-0.034%
$P_{t,2}$	-0.164%	-0.217%	0.010%
$P_{t,21}$	-0.201%	-0.225%	0.003%
$P_{t,24}$	0.027%	0.126%	0.241%
$P_{s,30}$	-0.739%	-0.752%	-0.372%
$P_{t,40}$	-1.219%	-0.859%	-0.573%
$P_{t,50}$	-0.362%	-0.436%	0.214%
N_f	-0.012%	0.000%	0.011%
N_c	-0.293%	-0.271%	-0.230%
W_f	1.429%	1.823%	2.134%

Table 3 – Final degradation values of performance parameters.

According to the degradation modes listed in Table 3, the three test engines mainly exhibit performance degradation in the high-pressure turbine and low-pressure turbine, namely decreases in turbine efficiency and flow capacity. From the perspective of aero-engine operating mechanisms, high-temperature gas expands and performs work in the turbine. When turbine efficiency decreases, the turbine work output per unit mass flow of gas decreases. When turbine flow capacity decreases, the flow-passing capability of the turbine is reduced, and the expansion process is affected, which also leads to a decrease in turbine work capacity. To maintain engine speed or thrust, the control system usually needs to increase the fuel flow rate. An increase in fuel flow raises the combustor outlet total temperature, thereby increasing the inlet temperatures of both the high-pressure turbine and the low-pressure turbine. Meanwhile, due to the reduction in turbine efficiency, the temperature drop across the turbine decreases; therefore, the outlet total temperatures of the high-pressure turbine and low-pressure turbine also increase accordingly. The above mechanism can explain the gradual increases in $T_{t,48}$, $T_{t,50}$, and W_f with operating time.

From the performance degradation assessment results, the high-pressure turbine outlet total temperature, low-pressure turbine outlet total temperature, and fuel flow all show clear increasing trends. This variation pattern is consistent with the theoretical analysis based on aero-engine operating principles and also agrees with the mechanistic characteristics of actual aero-engine performance degradation. These results indicate that the proposed degradation assessment method can effectively monitor aero-engine performance degradation.

5. Conclusions

This study proposes a real-time aero-engine performance degradation monitoring method under varying operating conditions. The method constructs a Baseline-State Model (BLS Model) and a Real-time Performance Model to reconstruct the healthy baseline performance and estimate the real-time operating performance under the same operating condition, respectively. Both models incorporate physical topology constraints and BiLSTM-based temporal feature extraction, while the Real-time model further introduces a self-attention mechanism to enhance component-level degradation representation.

A case study on the NASA N-CMAPSS DS02 subset shows that the average prediction errors of the BLS Model are below 0.2% on the first ten flight cycles of the three test engines. For full-life-cycle prediction, the Real-time model achieves average prediction errors below 0.3% on test engine No. 11, No.15and below 0.4% on the No.14. The calculated degradation trends are consistent with the actual degradation patterns of aero-engines, demonstrating the effectiveness and feasibility of the proposed method for real-time performance degradation monitoring.

6. Contact Author Email Address

Mail to: 2021100683@mail.nwpu.edu.cn

7. Copyright Statement

The authors confirm that they, and/or their company or organization, hold copyright on all of the original material included in this paper. The authors also confirm that they have obtained permission, from the copyright holder of any third party material included in this paper, to publish it as part of their paper. The authors confirm that they give permission, or have obtained permission from the copyright holder of this paper, for the publication and distribution of this paper as part of the ICAS proceedings or as individual off-prints from the proceedings.

References

[1] Ranier Kurz and Klaus Brun. Gas turbine tutorial-maintenance and operating practices effects on degradation and life. 2007.

[2] José Miguel Gil-García, Alejandro Solís, Gerardo Aranguren, and Joseba Zubia. An architecture for online measurement of the tip clearance and time of arrival of a bladed disk of an aircraft engine. *Sensors*, 17(10):2162, 2017.

[3] Pingping Yang, Wenhui Yue, Jian Li, Guangfu Bin, and Chao Li. Review of damage mechanism and protection of aero-engine blades based on impact properties. *Engineering Failure Analysis*, 140:106570, 2022.

[4] Maria Grazia De Giorgi, Nicola Menga, and Antonio Ficarella. Exploring prognostic and diagnostic techniques for jet engine health monitoring: a review of degradation mechanisms and advanced prediction strategies. *Energies*, 16(6):2711, 2023.

[5] Qian Chen, Hanlin Sheng, and Tianhong Zhang. A novel direct performance adaptive control of aero-engine using subspace-based improved model predictive control. *Aerospace Science and Technology*, 128:107760, 2022.

[6] LI Zhen, Shisheng Zhong, and LIN Lin. An aero-engine life-cycle maintenance policy optimization algorithm: Reinforcement learning approach. *Chinese journal of Aeronautics*, 32(9):2133–2150, 2019.

[7] Bin Zhang, Shaohui Zhang, and Weihua Li. Bearing performance degradation assessment using long short-term memory recurrent network. *Computers in industry*, 106:14–29, 2019.

[8] Dimitrios T Hountalas. Prediction of marine diesel engine performance under fault conditions. *Applied thermal engineering*, 20(18):1753–1783, 2000.

[9] Shuo Wang, Liang Yan, Shichang Du, Shanshan Li, and Xianmin Chen. Bearing prognostics and health management based on hybrid physical mechanism and data models: a systematic review. *Measurement Science and Technology*, 36(5):052002, 2025.

[10] Andrea Coraddu, Miltiadis Kalikatzarakis, Gerasimos Theotokatos, Rinze Geertsma, and Luca Oneto. Physical and data-driven models hybridisation for modelling the dynamic state of a four-stroke marine diesel engine. In *Engine Modeling and Simulation*, pages 145–193. Springer, 2021.

[11] Jeffryes W Chapman, Thomas M Lavelle, and Jonathan S Litt. Practical techniques for modeling gas turbine engine performance. In *52nd AIAA/SAE/ASEE joint propulsion conference*, page 4527, 2016.

[12] Di Wu, Donghuan Wang, and Hong Xiao. Nonlinear dissipation and nonequilibrium gas flows. *Physical Review E*, 100(3):032101, 2019.

[13] Hong Xiao, Yang-Yang Shi, Zhe-Zhu Xu, Lae-Sung Kim, Dong-yang Li, and Sung-Ki Lyu. Atomization characteristics of gelled hypergolic propellant simulants. *International Journal of Precision Engineering and Manufacturing*, 16(4):743–747, 2015.

[14] Hong Xiao, Zhe-Zhu Xu, and Sung-Ki Lyu. Quasi-steady-state scheme and application on prewhirl flow and heat transfer in aeroengine. *International Journal of Precision Engineering and Manufacturing*, 16(2):343–350, 2015.

[15] Ahmed Zohair Djeddi, Ahmed Hafaifa, Nadji Hadroug, and Abdelhamid Iratni. Gas turbine availability improvement based on long short-term memory networks using deep learning of their failures data analysis. *Process Safety and Environmental Protection*, 159:1–25, 2022.

[16] Dasheng Xiao, Zhifu Lin, Aiyang Yu, Ke Tang, and Hong Xiao. Data-driven method embedded physical knowledge for entire lifecycle degradation monitoring in aircraft engines. *Reliability Engineering & System Safety*, 247:110100, 2024.

[17] Dasheng Xiao, Hong Xiao, Rui Li, and Zhanxue Wang. Application of physical-structure-driven deep learning and compensation methods in aircraft engine health management. *Engineering Applications of Artificial Intelligence*, 136:109024, 2024.

[18] Chuming Gao, Zilang Huang, Aiyang Yu, Hong Xiao, and Zhishu Zhang. Similarity theory-driven dimensionless parameter migration framework: Digital twin approach for cross-condition gas turbine performance monitoring. *Applied Thermal Engineering*, page 129712, 2026.

[19] Chenchen Song, Hao Shi, Hong Xiao, and Aiyang Yu. Aircraft engine performance prediction via a physics-informed two-stage network framework. *Aerospace Science and Technology*, page 112051, 2026.

[20] Klaus Greff, Rupesh K Srivastava, Jan Koutník, Bas R Steunebrink, and Jürgen Schmidhuber. Lstm: A search space odyssey. *IEEE transactions on neural networks and learning systems*, 28(10):2222–2232, 2016.

[21] Ashish Vaswani, Noam Shazeer, Niki Parmar, Jakob Uszkoreit, Llion Jones, Aidan N Gomez, Łukasz Kaiser, and Illia Polosukhin. Attention is all you need. *Advances in neural information processing systems*, 30, 2017.